A Journal of the Gesellschaft Deutscher Chemiker

Angewandte International Edition GDCh Chemie

www.angewandte.org

## Accepted Article

**Title:** Fluorescence Imaging of Mitochondrial DNA Base Excision Repair Reveals Dynamics of Oxidative Stress Responses

**Authors:** Yong Woong Jun, Eddy Albarran, David L. Wilson, Jun Ding, and Eric T. Kool



**To be cited as:** *Angew. Chem. Int. Ed.* 10.1002/anie.202111829

**Link to VoR:** https://doi.org/10.1002/anie.202111829

WILEY-VCH

10.1002/anie.202111829

WILEY-VCH

RESEARCH ARTICLE

# Fluorescence Imaging of Mitochondrial DNA Base Excision Repair Reveals Dynamics of Oxidative Stress Responses

Yong Woong Jun,[a] Eddy Albarran,[b] David L. Wilson,[a] Jun Ding,[b] and Eric T. Kool*[a]

[a] Dr. Y. W. Jun, Dr. D. L. Wilson, and Dr. Prof. E. T. Kool
Department of Chemistry, ChEM-H Institute, and Stanford Cancer Institute
Stanford University
Stanford, California, 94305, United States
E-mail: kool@stanford.edu

[b] E. Albarran, and Dr. Prof. J. Ding
Department of Neurosurgery, Department of Neurology and Neurological Sciences, and Wu Tsai Neuroscience institute
Stanford University School of Medicine
Stanford, California, 94305, United States

Supporting information for this article is given via a link at the end of the document.

**Abstract:** Mitochondrial function in cells declines with aging and with neurodegeneration, due in large part to accumulated mutations in mitochondrial DNA (mtDNA) that arise from deficient DNA repair. However, measuring this repair activity is challenging. Here we employ a molecular approach for visualizing mitochondrial base excision repair (BER) activity *in situ* by use of a fluorescent probe (**UBER**) that reacts rapidly with AP sites resulting from BER activity. Administering the probe to cultured cells revealed signals that were localized to mitochondria, enabling selective observation of mtDNA BER intermediates. The probe showed elevated DNA repair activity under oxidative stress, and responded to suppression of glycosylase activity. Furthermore, the probe illuminated the time lag between the initiation of oxidative stress and the initial step of BER. Absence of MTH1 in cells resulted in elevated demand for BER activity upon extended oxidative stress, while the absence of OGG1 activity limited glycosylation capacity.

## Introduction

Genetic information in mammalian cells is stored in two repositories: nuclei and mitochondria.[1] Nuclear DNA (nDNA) in a human cell contains 3.3 billion base pairs (bp), distributed among 46 chromosomes and harboring 20,000–25,000 protein-coding genes.[2] In contrast, mitochondrial DNA (mtDNA) is a circular gene-dense supercoiled molecule of ca. 16,500 bp, which encodes two rRNAs, 22 tRNAs, and 13 polypeptides, and comprises 0.1–2% of cellular DNA by mass.[3] While the importance of mutations that arise in nDNA is widely recognized, mtDNA mutations, which can compromise mitochondrial function, have also been implicated in over 200 disorders including aging,[4] cancer progression,[5] and neurodegenerative disorders.[6] Mutations in mtDNA occur 10–20 times more frequently than in nDNA both due to the lack of protective histones and to the mitochondrial electron transport chain that generates DNA-damaging reactive oxygen species (ROS).[7] Moreover, mtDNA, which replicates throughout the cell cycle (the entire cycle takes only ~2 hr and even persists in nondividing cells)[8], accumulates mutations approximately one order of magnitude more rapidly than nDNA.[9]

The major DNA repair mechanism in mitochondria is base excision repair (BER).[10] The critical first step of BER begins with the recognition and removal of a damaged nucleobase by a damage-specific glycosylase enzyme, creating an apurinic/apyrimidinic (AP) site.[11] This is subsequently cleaved by a lyase activity, and the resulting one-base gap is filled in by polymerase and ligase activities to complete the repair process.[7a] Given the high frequency of DNA-damaging events — estimated at over 10,000 events per cell per day[12] — the DNA repair pathways in mitochondria can be overwhelmed, with serious consequences. As such, maintaining the integrity of mtDNA via active repair is essential for healthy life, and studies of mtDNA damage and its repair have significant relevance to human health.

Classical methods for quantifying DNA damage and measuring DNA repair activity have included the quantification of DNA lesions by mass spectrometry, isotope-dilution methods, quantitative polymerase chain reaction (qPCR) methods from isolated cellular DNA,[13] and measurements using an oligonucleotide containing a damaged base with a DNA repair enzyme extracted from cells or tissues.[14] The methods all require isolation and multi-step analysis, and thus are relatively slow and labor-intensive. In addition, the studies are performed outside of their biological context, which can result in inaccuracies; for example, it has been shown that common DNA lesions such as 8-oxo-7,8-dihydro-2'-deoxyguanine (8-oxo-dG) can arise as an artifact during sample preparation.[15] In general, *in vitro* measurements of glycosylase activity can be biased by not accurately representing enzymatic function *in vivo*, considering that many glycosylase enzymes do not turn over *in vitro*, while they do so in living systems by interacting with other cellular components.[16] Thus, there remains an unmet need for simpler and more direct methods of measuring DNA repair activity, particularly in the mitochondrial context where damage and mutations are elevated. In addition, the availability of an *in situ* method for observing DNA repair responses could enable the first measurements of dynamics of the damage response processes.

Herein, we describe a novel strategy for visualizing mtDNA BER activity in living cells by a cell-permeable small-molecule fluorescent probe. We find that the probe, **UBER** (universal base excision reporter, Figure 1a), recently shown to react with AP sites in DNA *in vitro*,[17] is cell permeable and responds to enzymatic base excision in mtDNA of living cells via a robust light-up response. We further report that the probe is two-photon-active,

10.1002/anie.202111829




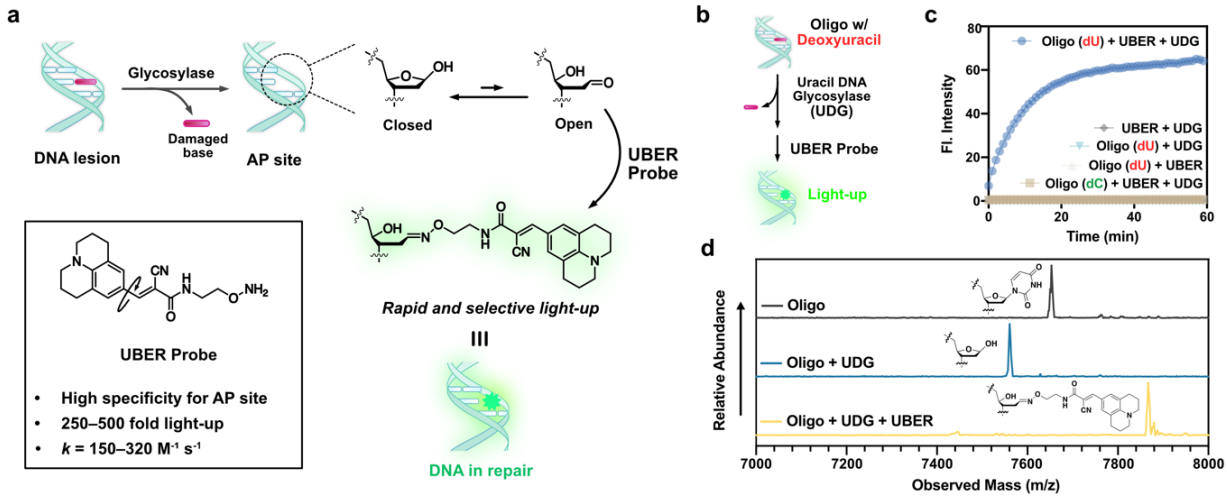


**Figure 1.** (a) Chemistry of **UBER** green fluorescent probe reacting with the aldehyde form of the AP site in DNA, and the chemical structure of the **UBER** probe, containing a dark rotor dye that lights up when constrained by reaction in DNA. (b) Scheme of *in vitro* test of **UBER** binding to an AP site generated by UDG which removes uracil in DNA. (c) Fluorescence real-time responses of **UBER** (10 $\mu$M) with oligonucleotides (1 $\mu$M) containing deoxyuridine or deoxycytidine in the presence or absence of UDG (10 U/mL). (d) MALDI-TOF spectra of the oligonucleotides used in the *in vitro* tests, confirming covalent reaction with AP-containing DNA.

enabling convenient imaging in tissue sections. This readily-implementable approach visualizes the real-time activity of the mtDNA BER process in native cellular and tissue environments under varied conditions such as oxidative stress and drug-mediated inhibition. With this approach, we explore the elevation and timing of the DNA repair responses upon the induction of exogenous DNA damage, and we correlate responses to the roles of two major DNA repair enzymes.

## Results and Discussion

We considered the possibility that measurement of mtDNA BER activity in living cells might be achieved by detecting AP sites, which are critical intermediates in BER. The technical challenge of this goal has been that previously reported aldehyde reactive probes (ARP) labelling AP sites with aminooxy-functionalized fluorophores and affinity tags do not engender a light-up or fluorogenic response.[19] Moreover, they react well with aldehyde interferents that are present in cells. As a result, utilization of such probes in cells has been limited to quantification of AP sites from isolated DNA by gel-based assays rather than real-time visualization in the native context. Toward this goal, we tested the reactive **UBER** probe (green "CCVJ1" variant[17]), which undergoes highly selective and rapid oxime formation with the aldehydic form of AP sites in DNA (Figure 1a) and affords a high fluorescence enhancement that obviates the need for isolation or washing steps. To assess the formation of covalent binding of **UBER** to AP sites and the light-up response, we prepared an oligonucleotide containing a single deoxyuracil (Figure 1b). Addition of uracil DNA glycosylase (UDG) to a mixture of the oligonucleotide and **UBER** (10 $\mu$M) yielded >200-fold fluorescence enhancement within 20 min (Figure 1c). When the deoxyuracil in the oligonucleotide was replaced by deoxycytosine, which is not a substrate for UDG, no light-up signal was observed. MALDI-TOF analysis of the reacted oligonucleotide after UDG/**UBER** documented covalent bond formation with the AP site with almost full conversion (Figure 1d).

Not only the aldehyde but also the cavity defined by the missing base in an AP site plays a critical role in the detection. The cavity provides the proximity effect to the planar portion of **UBER** which markedly accelerates the oxime formation, and results in a highly constrained environment which affords high quantum yields.[17] To evaluate the importance of the AP site cavity, a set of small-molecule aldehydes was tested with **UBER**, but none afforded fluorescence enhancement (Figure S1). In addition, **UBER** detected AP sites even in the presence of high levels of glucose (500 equiv.) that also contain the aldehyde moiety in equilibrium without any kinetic compromise (Figure S2). Lastly, other aldehydic lesions such as 5'-aldehyde generated at DNA strand breaks afforded very low enhancement (Figure S3). The role of the cavity in AP sites enables selective detection of AP sites in cells which contain many potential interferents. We note also that while endogenous AP sites are formed both by glycosylase activity and spontaneous depurination that is dependent on pH and temperature,[18] the glycosylase activity is likely primarily responsible for the fluctuation of AP site levels inside cells where pH and temperature are constant.

Initial tests involving simple incubation of the probe with HeLa cells resulted in punctate green signals observable within an hour by confocal microscopy (Figure 2a, Figure S4). Note that previous studies of mtDNA replication using bromo-deoxyuridine (BrdU) with antibody staining in fixed cells also showed similarly located punctate signals.[20] Intracellular localization of **UBER** signals was examined by co-labeling with Hoechst 33342 (nucleus, blue) and MitoTracker DR (mitochondria, red) to evaluate intracellular locations of the new signals relative to nuclear or mitochondrial DNA (Figure 2b). Colocalization analysis indicated that **UBER** co-localizes with the mitochondrial dye (PCC = 0.872), while it does not overlap with Hoechst (Figure 2c). Images overlaid with a ~0.5 µm of vertical offset confirmed that green fluorescent signals from **UBER** always appeared in the spots where mitochondria are located (Figure 2d). A distinctive feature of **UBER** in this imaging is that it shows different fluorescence intensities in each mitochondrion (marked with arrows in cyan and yellow), while MitoTracker stains most mitochondria fairly evenly (Figure 2e). This result implies that **UBER** is not simply localized in

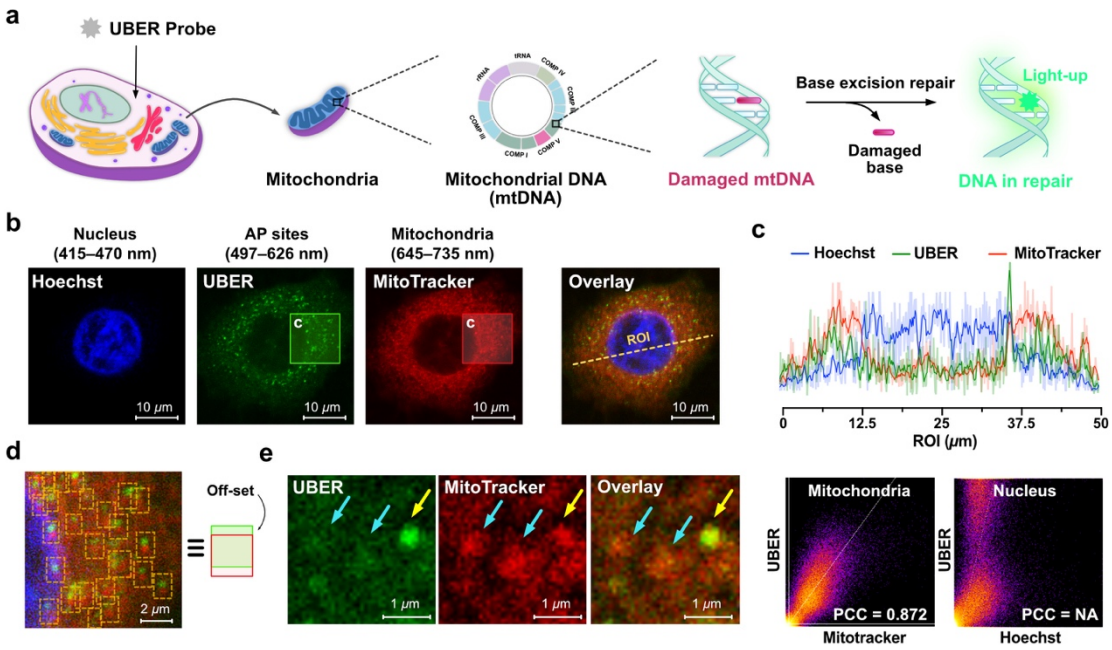


**Figure 2.** (a) Schematic description of **UBER** probe binding to the lesion in mitochondrial DNA and affording fluorescence signal. (b) Confocal fluorescence images of Hoechst 33342, **UBER**, and MitoTracker DR in HeLa cells. (c) Histogram of fluorescence intensity extracted from the overlaid image in Figure 2b and colocalization coefficient plots of **UBER** with MitoTracker and Hoechst. (d) Images overlaid with a vertical off-set from Figure 2b. (e) Magnified images showing three mitochondria. Hoechst (10 $\mu$g/mL, $\lambda_{ex}$ = 405 nm, $\lambda_{em}$ = 415–470 nm, $t_{inc}$ = 30 min), **UBER** (10 μM, $\lambda_{ex}$ = 488 nm, $\lambda_{em}$ = 497–626 nm, $t_{inc}$ = 5 h), MitoTracker DR (500 nM, $\lambda_{ex}$ = 633 nm, $\lambda_{em}$ = 645–735 nm, $t_{inc}$ = 30 min).

mitochondria due to its chemical structure, but rather suggests that the probe responds to differential biology of distinct mitochondria. This differing fluorescence intensity in mitochondria is also consistent with the known heteroplasmy of mtDNA,[21] which results in varied levels of function among different mitochondrial compartments within a cell (Figure S5).

It is interesting to note that **UBER** shows very little fluorescence response localized to nuclei under the conditions studied here, despite the fact that much more DNA is present in the nucleus relative to mitochondria. One possible explanation includes potentially poor nuclear membrane penetrance by the small molecule probe. To evaluate this possibility, we fixed and permeabilized the cells, then treated with probe and imaged the fluorescence signal (Figure S6). In this case, the **UBER** signal was observed from the nucleus as well as mitochondria, which adds evidence that nuclear membrane permeability of the probe is a limiting factor in intact cells.

While the mitochondrial localization of **UBER** signals along with its known DNA-selective reactions are suggestive of labeling of AP sites in mtDNA, more evidence was needed of this hypothesized response. As a positive control, cells were exposed to an oxidant ($KBrO_3$) that is known to generate reactive radical species inducing oxidative damage to cellular DNA, in particular, elevating levels of 8-oxo-dG (Figure S7).[22] This lesion is known to be excised exclusively by the mitochondrial isoform of the enzyme OGG1.[23] Analysis by flow cytometry showed that HeLa cells under oxidative stress exhibited stronger fluorescence signals from **UBER** (Figure 3a,b), plausibly due to the enhanced mtDNA repair activity in the presence of elevated levels of oxidative damage. Note that the generation of radical species by $KBrO_3$ in the absence of DNA outside of cells caused negligible fluorescence enhancement of the probe (Figure S8). In addition, mtDNA pellets isolated from the cells incubated with **UBER** exhibited higher signals when the cells underwent oxidative stress (Figure S9), adding direct evidence of association of the probe with the mtDNA itself. The **UBER** imaging experiment was further evaluated in SW620 and SW480 colorectal cancer cell lines to test generality of the observations. Metastatic SW620 cells are reported to have a higher mtDNA copy number than do primary SW480 cells.[24] Consistent with this, **UBER** exhibited a higher fluorescence intensity in SW620 cells and the treatment of $KBrO_3$ showed a greater extent of enhancement in SW620 (Figure 3c). These observations support the capability of the **UBER** probe for detecting AP sites that arise from oxidative damage and repair in mtDNA.

As negative control experiments, mtDNA repair activity was reduced in two ways: by lowering the number of DNA lesions, and by suppressing repair activities. 8-oxo-dG, the most common form of oxidative damage in DNA,[25] either arises directly in DNA or can be incorporated by a polymerase into mtDNA in the form of the damaged nucleotide 8-oxo-dGTP.[26] DNA polymerase gamma (Pol$\gamma$) is believed to be solely responsible for mtDNA synthesis.[27] The repair of the mtDNA lesion once incorporated into DNA is carried out by OGG1, the primary enzyme responsible for the excision of oxidized guanine lesions. We first tested the Pol$\gamma$ inhibitor 2',3'-dideoxycytidine (ddC) with HeLa cells in order to reduce the incorporation of oxidatively damaged nucleotides into mtDNA.[28] Consistent with our hypothesis, flow cytometric analysis showed lower signals with **UBER** upon the addition of ddC in dose-dependent manner (Figure 3d), which we attribute to decreased mtDNA damage levels as a result of lowered incorporation of damaged nucleotides. Additionally, we demonstrated a mtDNA-selective damage reduction by using a mitochondrial uncoupling reagent, BAM15. Mitochondrial superoxide production is steeply dependent on the electrochemical proton gradient. Correspondingly, mitochondrial uncoupling has been identified as a cytoprotective strategy that is able to protect against mitochondrial oxidative damage by

10.1002/anie.202111829




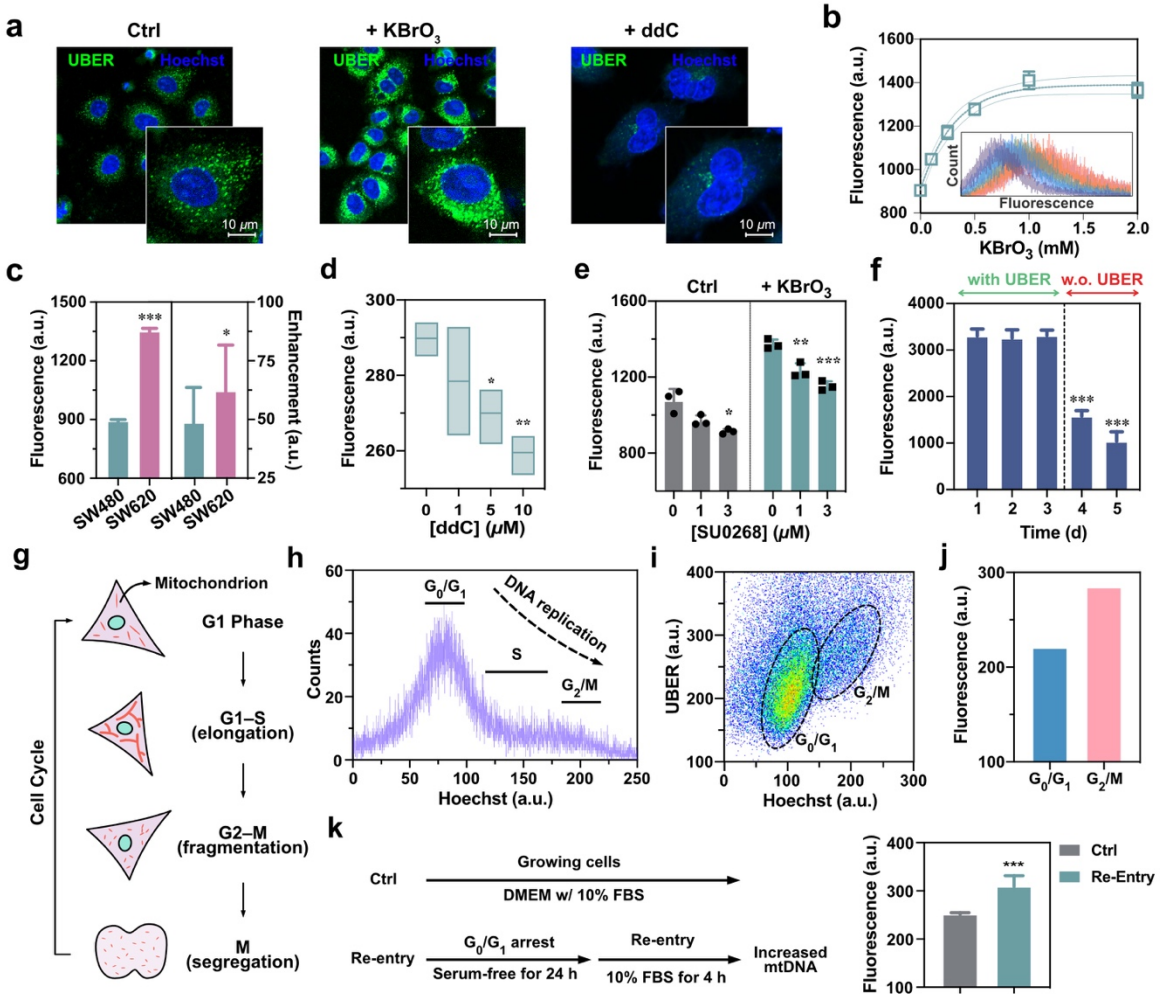


**Figure 3.** (a) Confocal images of control cells, oxidatively stressed cells with $KBrO_3$, and mtDNA-depleted cells treated with ddC, after washing unreacted probe out. (b) Flow cytometric analysis showing the fluorescence intensities depending on the concentration of $KBrO_3$ in the cellular media. (c) Flow cytometric analysis data of colorectal cancer cells (left) and enhancement under oxidative stress (right). (d) Flow cytometry data of mtDNA repair activity measured in HeLa cells by **UBER** upon the addition of ddC for 2 days. (e) mtDNA repair activity measured in HeLa cells by **UBER** upon the addition of OGG1 inhibitor SU0268 under normal vs. oxidative stress conditions. (f) Fluorescence intensity in cellular media after removing **UBER** from the media. (g) Illustration of mitochondrial dynamics during the cell cycle. (h) Cell cycle analysis with **UBER**: FACS analysis data of HeLa cells stained with Hoechst (5 $\mu$g/mL) for an hour indicating the amount of DNA in each cell. (i) FACS analysis data showing the relative intensities of **UBER** (10 $\mu$M) and Hoechst in each cell. (j) Fluorescence intensity comparison of **UBER** in $G_0/G_1$ cells and $G_2$/M cells. (k) Preparation process of the cells with stimulated mitochondrial biogenesis, and the fluorescence intensity of **UBER** (10 $\mu$M) in growing and stimulated HeLa cells. Fluorescence intensity was collected at 530 nm with excitation at 488 nm. [**UBER**] = 10 $\mu$M, [Hoechst] = 10 $\mu$g/mL, [$KBrO_3$] = 2 mM. Incubation time: 48 h (ddC) and 24 h (SU0268). $\lambda_{ex}$ = 405 nm (Hoechst), 488 nm (**UBER**), $\lambda_{em}$ = 410–450 nm (Hoechst) and 500–800 nm (**UBER**).

reducing the production of ROS.[29] Treatment with BAM15 higher than 5 $\mu$M for 5 h resulted in lowered fluorescence intensities of **UBER** (Figure S10), which is consistent with the previous reports that mitochondrial uncoupling reduces the production of ROS and corresponding oxidative damage in mitochondria.

Secondly, the oxidative damage-specific glycosylation activity in HeLa cells was attenuated by treatment with a potent OGG1 inhibitor, SU0268 (IC50 = 0.059 $\mu$M), for 24 h (Figure 3e).[30] Upon incubation with SU0268, HeLa cells exhibited decreased fluorescence intensity under both normal and oxidative stress conditions, which indicates reduced 8-oxo-dG base excision activity as expected. Taken together, the AP site-selective light-up response of **UBER**, the mitochondrial localization of signals and association with isolated mtDNA, the responses to oxidative stress and to multiple enzyme inhibition, all support the notion that the **UBER** probe reacts with and generates signals at AP sites that arise in mtDNA as a result of damage excision.

One question that arose during our early experiments was the issue of repairability of **UBER** adducts in mtDNA. Since **UBER** forms relatively stable covalent bonds with AP sites, the addition of **UBER** to the cells might lead to the accumulation of the covalent probe in mtDNA, which could be mutagenic or toxic unless the adduct is repairable by cellular repair processes. Incubating 10 $\mu$M **UBER** in the cell culture media for an extended period of three days did not show any further accumulation of **UBER** in the cells (Figure 3f), which shows that it reaches a steady state of incorporation into mtDNA and removal from the DNA without overt cytotoxicity (Figure S11). *In vitro* study with cytosolic cellular lysate containing mitochondrial BER proteins documented the repair activity toward **UBER** labeled AP sites (Figure S12). Once the probe was removed from the media, the fluorescent signal diminished over the subsequent two days (Figure 3f). The results imply that the **UBER** adduct is eventually

10.1002/anie.202111829
WILEY-VCH

RESEARCH ARTICLE

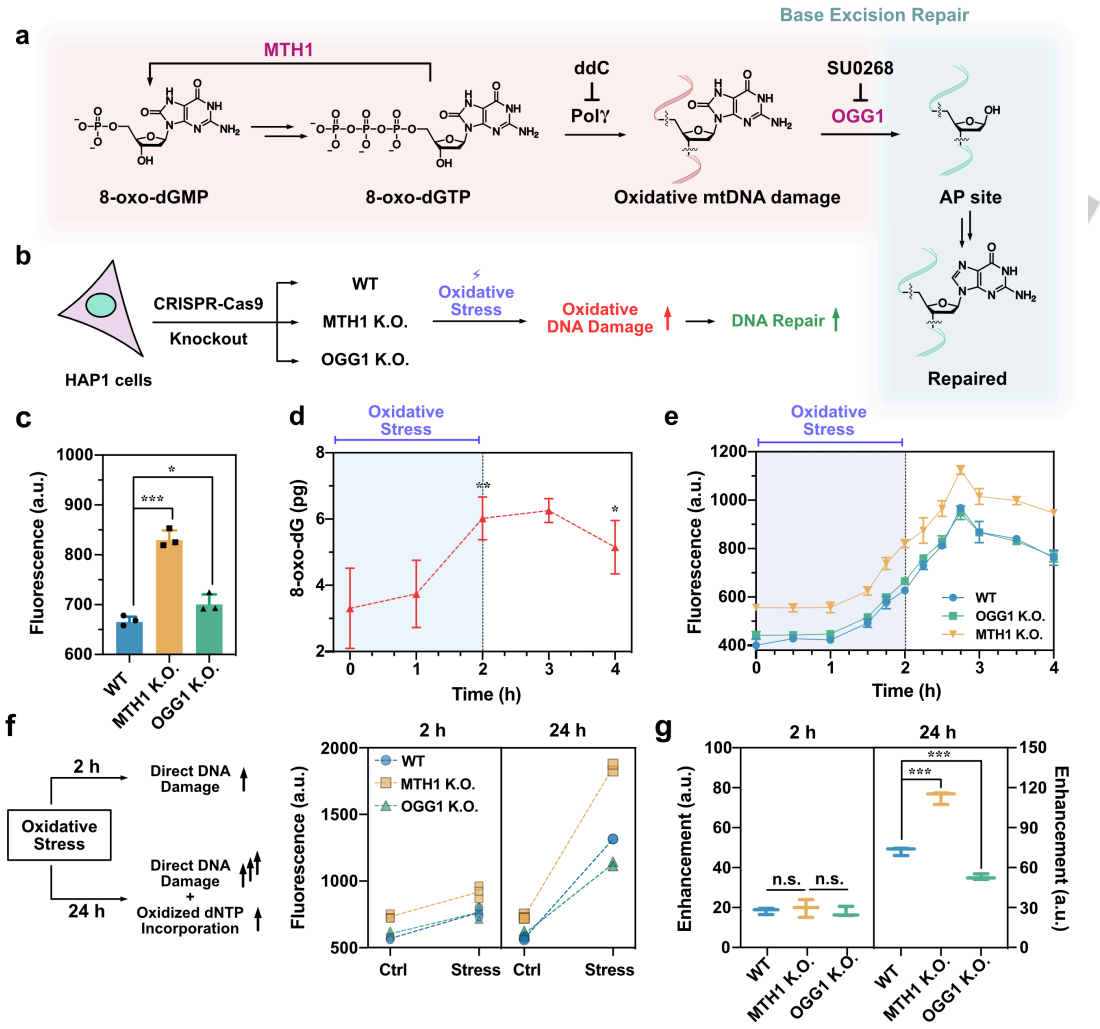


**Figure 4.** (a) Scheme of the incorporation of 8-oxo-dGTP into mtDNA and its repair by BER process. (b) Experimental setup for evaluating the effect of two DNA repair enzymes under oxidative stress. (c) mtDNA repair activity comparison in three HAP1 cell lines: Wild-type, MTH1 KO, and OGG1 KO. (d) Changes in the amount of 8-oxo-dG in the cellular DNA quantified by ELISA, after oxidative stress for 2 h. (e) DNA repair activity change under oxidative stress. (f) DNA repair activity under oxidative stress for 2 h and 24 h. (g) Fluorescence enhancement comparison in three HAP 1 cells lines under oxidative stress for 2 h and 24 h. [**UBER**] = 10 $\mu$M, [$KBrO_3$] = 2 mM

removed from mtDNA, and then cannot be re-incorporated into the DNA.

Mitochondria fuse and elongate during the G1–S transition, then undergo fission, fragmentation, and segregation at G2 and M phases (Figure 3g).[31] To investigate how the fluorescence signal is influenced during mitosis, cell cycle analysis with **UBER** probe was carried out. We employed Hoechst 33342 to correlate the fluorescence signal from **UBER** with the amount of DNA at different phases of the cell cycle. As the DNA content doubles during the mitosis, cells in different phases mark their cell-cycle phase by the relative Hoechst intensity indicating the amount of DNA (Figure 3h). **UBER** afforded higher fluorescence intensity in the cells in $G_2$/M phase, which is consistent with the fact that the mitochondria replicate their DNA prior to cell division (predominantly in the late S and $G_2$ phases, Figure 3i,j).[32] To further confirm that the biogenesis of mitochondria (and mtDNA) contributes to the increase of **UBER** signal, we synchronized HeLa cells in $G_0/G_1$ phases by culturing in serum-free media for 24 h, then mitochondrial biogenesis was stimulated by exchanging the media with 10% FBS containing media. It has been reported that when synchronized cells re-enter the cell cycle, the copy number of mtDNA increases > 1.5-fold at 4 h after the re-entry.[33] Consistent with the previous observation, the synchronized cells showed higher fluorescence intensity from **UBER** at 4 h after re-entry (Figure 3k).

We employed **UBER** to further explore the effect of OGG1 and another front-line defensive enzyme against oxidative DNA damage, namely MTH1 encoded by the *NUDT1* gene. MTH1 binds to 8-oxo-dGTP and hydrolyzes its triphosphate moiety between α and β phosphates, preventing its incorporation into DNA (Figure 4a).[34] In the experimental setup, two knockout (KO) HAP1 cell lines by CRISPR-Cas9 were studied (HAP1 wild type, MTH1-knockout, and OGG1-knockout, Figure 4b). Deficiency in each of these enzymes is known to increase susceptibility to oxidative damage in cellular DNA.[35] The chief difference between the MTH1 and OGG1 KO cell lines is expected to be the glycosylation capacity: the OGG1-deficient cell line is expected to have reduced glycosylation capacity, while the MTH1-deficient cells should have full glycosylation capacity.

Flow cytometric analysis with **UBER** shows that the MTH1 knockout cell line exhibits a higher mtDNA base excision activity than WT, as might be expected due to the elevated levels of oxidatively damaged nucleotides entering DNA from the nucleotide pool (Figure 4c). Interestingly, the OGG1 KO cell line

showed slightly higher mtDNA repair levels (as indicated by **UBER**) than WT HAP cells, despite of the absence of OGG1 which is one of the major glycosylases. We hypothesize that other repair glycosylases likely compensate for the absence of OGG1 quite efficiently, which in aggregate are able to cover mtDNA damage when it is not severe. As a result, higher DNA damage in OGG1 KO cells resulted in a mildly elevated level of AP sites. We speculate that the absence of OGG1 is likely rescued by Nei-like1–3 (NEIL1–3) and/or MutYH glycosylases, which are responsible for the repair of the hydantoin products related to 8-oxo-dG and adenine bases inappropriately paired with 8-oxo-dG, respectively.[36]

Next, we explored whether the absence of these enzymes affected the kinetics of the cellular response to oxidative damage; **UBER**'s cell permeability, fast reaction and light-up response would make such measurements possible. Although kinetics methods for *in vitro* study of DNA repair enzymes are well established,[37] methods for observing repair processes in cells over time are quite limited.[38] To evaluate the kinetics of DNA repair activation after initiation of exogenous oxidative stress, HAP1 cell lines were exposed to $KBrO_3$ for 2 h, then the changes of DNA damage and repair activity were observed over time. As a substrate of DNA repair, oxidative DNA damage was monitored by quantifying the concentration of 8-oxo-dG in the isolated cellular DNA by ELISA at different time points. As reported, the 8-oxo-dG increased over time upon the addition of $KBrO_3$ (Figure 4d).[39] The concentration of 8-oxo-dG reached a plateau, while cells remained under the oxidative stress, and began to decrease 1 h after the oxidant was removed from the culture medium. On the other hand, DNA repair activity as measured by **UBER** began to increase after the cells underwent oxidative stress for 1.5 h, and reached a peak ca. 45 min after the oxidant was removed; signals then decreased rapidly (Figure 4e). The results point to the time lag between the exogenous DNA damage caused by the oxidant and the subsequent elevation of DNA repair activity. Previous studies have observed that *in vitro* exposure to ROS activates a sophisticated network of DNA damage-response systems;[40] however, it has not previously been possible to observe the timing of this activation in real time. It is interesting that all three cell lines under these relatively mild oxidative conditions showed little or no difference in the kinetics and extent of DNA repair activity enhancement.

To evaluate the effect of these defensive enzymes under conditions in which DNA damage is more pronounced, the oxidative stress was extended to 24 h for the three cell lines. In this more severe case, higher levels of direct DNA damage are expected, along with the increased incorporation of oxidized dNTP, where the role of MTH1 would play a role (Figure 4f,g). Under these conditions, the mtDNA base excision activity was greatly elevated in the MTH1 KO cell line, consistent with expectations and also consistent with prior observations that this cell line is more vulnerable to oxidative damage than is the WT line.[35] In the case of the OGG1 KO cell line, mtDNA base excision activity appeared to be enhanced the least. Given that the OGG1 KO cell line is expected to undergo similar or higher levels of DNA damage than in WT cells, the lower glycosylation activity of the OGG1 KO cell line appears to be insufficient to cope with the oxidative damage. The results can be explained by the attenuated glycosylation capacity; under this extensive oxidative stress, cells lacking OGG1, the major glycosylase combating oxidative damage, appear to reach their limit of glycosylation capacity. Overall, under conditions where DNA damage is relatively mild, the absence of MTH1 or OGG1 was observed to be compensated for by other DNA repair enzymes. However, when the DNA damage is extensive, the absence of a nucleotide surveillance enzyme (e.g., MTH1) can lead to a need for higher DNA BER repair activity. In the absence of OGG1 activity, cells reach the effective limit of glycosylation, increasing the accumulation of DNA damage.

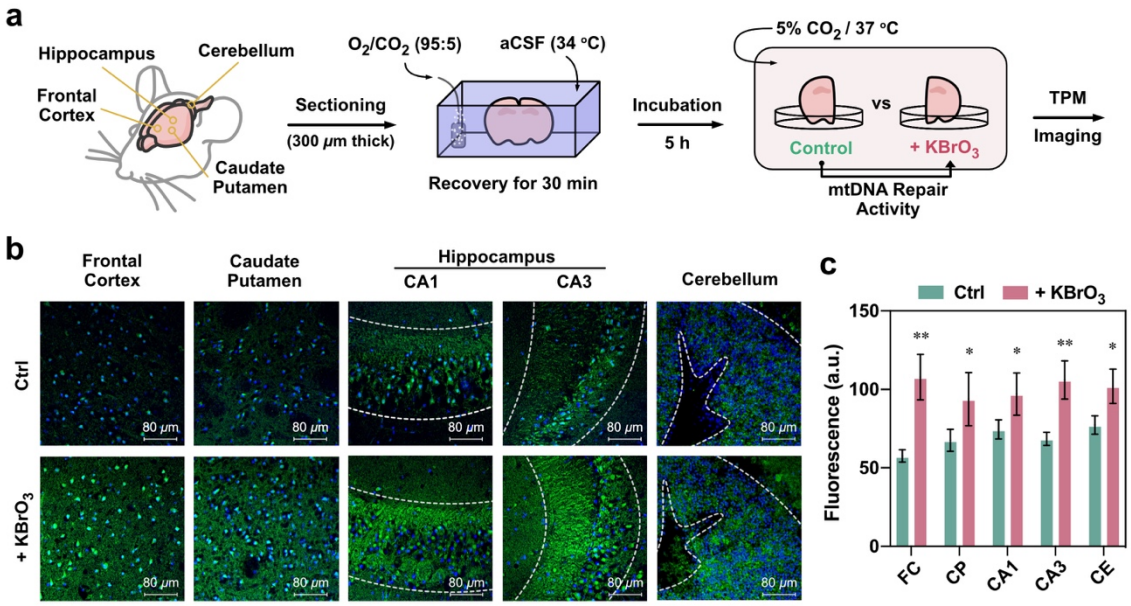


**Figure 5.** (a) Schematic procedure of the preparation and imaging of fresh mouse brain thin slices. (b) Visualized mtDNA repair activity in four regions of mouse brain (frontal cortex (FC), caudate putamen (CP), hippocampus (CA1 and CA3), and cerebellum (CE)) by two-photon microscopy. (c) Fluorescence intensity enhancement under oxidative stress (N = 3). [**UBER**] = 20 μM (for tissue), [Hoechst] = 10 μg/mL, [$KBrO_3$] = 10 mM (for tissue). Incubation time: 4.5 h. $\lambda_{ex}$ = 780 nm (Hoechst) and 950 nm (**UBER**), $\lambda_{em}$ = 410–450 nm (Hoechst) and 500–800 nm (**UBER**). Thickness of brain slices: 300 μm. Imaging depth: ~130 μm.

Given the **UBER** probe's responses to oxidative stress and to repair enzyme modulation, we next applied this system to measure mitochondrial DNA repair activity in living tissue. Importantly, we observed that the probe is two-photon excitable at 900–950 nm (Figure S13), which enables excitation in the biological absorption window maximizing tissue penetration and minimizing autofluorescence.[41] In addition, we observed very high photostability in the dye (Figure S14), which is a useful property for imaging carried out under high light intensity. Given that impaired mtDNA repair activity in the brain has been implicated in aging and neurodegenerative disorders,[42] visualizing mtDNA repair activity in the brain has the potential to be a powerful tool in the study of these pathologies. No such imaging is currently available. Measuring an analyte in tissue level using a fluorescent probe, however, can be easily biased by numerous factors affecting fluorescence intensity of the probe by the heterogeneous nature of tissue.[43] In order to compensate for factors that cause local variations in fluorescence signal such as microenvironment and local concentration, we adopted a new procedure, in which acute brain slices are hemi-sectioned, then one hemisphere is incubated with **UBER** under oxidative stress, while the other hemisphere is incubated with **UBER** under normal tissue-supportive conditions (Figure 5a). Direct comparison of these two mirror-image hemispheres compensates for non-specific fluorescence that disturbs the fluorescence signal from mtDNA repair activity, and allowed us to reliably measure the dynamic fluorescence enhancement due to glycosylation activity.

The acute brain sections were prepared from four distinct mouse brain regions, which are reported to have relatively high mtDNA repair activity in young animals (Figure 5a).[14] After the slices recovered from sectioning were bathed in artificial cerebrospinal fluid (aCSF) for 30 min to preserve the cellular physiology and activity of enzymes in the brain tissue, the slices were incubated with **UBER** and imaged under a two-photon microscope (Figure 5b). Brain slices incubated under oxidative stress displayed enhanced fluorescence intensity relative to basal signals (Figure 5c). Fluorescence enhancement in the frontal cortex was observed to be higher than that in the hippocampus (CA1 and CA3), which is consistent with previous reports, measured with mitochondrial extracts, that hippocampal mtDNA repair glycosylases exhibit lower activity when compared with preparations from the cortex.[44] One phenomenon that we noted in two-photon images of hippocampus is that fluorescence enhancement was significantly higher in the pyramidal layer and stratum radiatum (outlined by dotted lines), where pyramidal neuron cell bodies and their dendrites reside, respectively. This observation is consistent with early studies of oxidative damage repair enzymes in neural cells and tissues; the expression level of MutYH DNA glycosylase involved in the repair of oxidative damage was found to be increased in neural mitochondria in rats,[45] and OGG1 is reported to protect neurons against oxidative DNA damage.[46] The ability of **UBER** to measure and distinguish between variable levels of repair activity in different regions of the brain is a unique feature of this probe.

## Conclusions

We have described the unprecedented direct imaging of the spatiotemporal evolution of DNA damage exposure and repair in mitochondria. This was enabled by the cell-permeable small-molecule probe **UBER** (CCVJ1), detecting AP sites as they are formed by base excision. Co-localization analysis reveals that the majority of fluorescence signal localizes in mitochondria, and the probe responds over a period of hours to elevated damage arising from exogenous oxidants, resulting in enhanced fluorescence intensity, and reports on the effects of inhibitors of enzymes that contribute to damage and repair of mtDNA. The probe can distinguish between differential mitochondrial function and repair in distinct cell lines, and it can be employed both in imaging mode and quantified by flow cytometry. Further, we show that the probe is two-photon active with excitation at 950 nm, enabling convenient and detailed microscopic imaging of repair activity in fresh brain tissue with low background, and revealing different repair signals in distinct regions of the acute brain slices. Finally, we have employed **UBER** to observe dynamics of mtDNA damage and its repair, revealing relationships between cooperating repair pathways. Given that DNA repair processes involve many proteins that interact with each other intricately, DNA repair activities are arguably best and most accurately measured in the native context. Thus, the new **UBER** probe holds the potential to provide novel insights into mtDNA damage and repair biology as well as into the many pathologies that are associated with impaired mitochondrial function.

## Acknowledgements

We gratefully acknowledge support from the U.S. National Cancer Institute (R01 CA217809 to ETK) and NINDS/NIH (NS075136 to JBD), the Klingenstein Foundation (JBD), HHMI Gilliam Fellowship (EA), NSF GRFP (EA), and DARE Fellowship (EA).

**Keywords:** DNA damage • mitochondrial DNA • base excision repair • fluorescence probe • AP site

[1] L. Kazak, A. Reyes, I. J. Holt, *Nat. Rev, Mol. Cell Biol.* **2012**, *13*, 659–671.
[2] E. S. Lander, *Nature* **2011**, *470*, 187–197.
[3] N. M. Druzhyna, G. L. Wilson, S. P. LeDoux, *Mech. Ageing Dev.* **2008**, *129*, 383–390.
[4] A. Trifunovic, A. Wredenberg, M. Falkenberg, J. N. Spelbrink, A. T. Rovio, C. E. Bruder, M. Bohlooly-Y, S. Gidlöf, A. Oldfors, R. Wibom, *Nature* **2004**, *429*, 417–423.
[5] K. Ishikawa, K. Takenaga, M. Akimoto, N. Koshikawa, A. Yamaguchi, H. Imanishi, K. Nakada, Y. Honma, J.-I. Hayashi, *Science* **2008**, *320*, 661–664.
[6] Y. Xu, C. K. Phoon, B. Berno, K. D'Souza, E. Hoedt, G. Zhang, T. A. Neubert, R. M. Epand, M. Ren, M. Schlame, *Nat. Chem. Biol.* **2016**, *12*, 641–647.
[7] a) B. N. Ames, M. K. Shigenaga, T. M. Hagen, *Proc. Natl. Acad. Sci.* **1993**, *90*, 7915–7922; b) L. Zhao, P. Sumberaz, *Chem. Res. Toxicol.* **2020**, *33*, 2491–2502.
[8] D. Bogenhagen, D. A. Clayton, *Cell* **1977**, *11*, 719–727.
[9] W. M. Brown, M. George, A. C. Wilson, *Proc. Natl. Acad. Sci.* **1979**, *76*, 1967–1971.
[10] D. L. Croteau, V. A. Bohr, *J. Biol. Chem.* **1997**, *272*, 25409–25412.
[11] B. Karahalil, B. A. Hogue, N. C. de Souza-Pinto, V. A. Bohr, *FASEB J.* **2002**, *16*, 1895–1902.
[12] T. Lindahl, *Nature* **1993**, *362*, 709–715.
[13] a) N. Tretyakova, M. Goggin, D. Sangaraju, G. Janis, *Chem. Res. Toxicol.* **2012**, *25*, 2007–2035; b) S. Liu, Y. Wang, *Chem. Soc. Rev.* **2015**, *44*, 7829–7854; c) A. Furda, J. H. Santos, J. N. Meyer, B. Van Houten, in *Methods Mol. Biol., Vol. 1105*, Springer, **2014**, pp. 419–437.

[14] S. Z. Imam, B. Karahalil, B. A. Hogue, N. C. Souza-Pinto, V. A. Bohr, *Neurobiol. Aging* **2006**, *27*, 1129–1136.
[15] G. Boysen, L. B. Collins, S. Liao, A. M. Luke, B. F. Pachkowski, J. L. Watters, J. A. Swenberg, *J. Chromatogr. B* **2010**, *878*, 375–380.
[16] a) M. R. Baldwin, P. J. O'Brien, *Biochemistry* **2009**, *48*, 6022–6033; b) S. Ikeda, T. Biswas, R. Roy, T. Izumi, I. Boldogh, A. Kurosky, A. H. Sarker, S. Seki, S. Mitra, *J. Biol. Chem.* **1998**, *273*, 21585–21593.
[17] D. L. Wilson, E. T. Kool, *J. Am. Chem. Soc.* **2019**, *141*, 19379–19388.
[18] J. R. Fresco, O. Amosova, *Annu. Rev. Biochem.* **2017**, *86*, 461–484.
[19] a) K. Kubo, H. Ide, S. S. Wallace, Y. W. Kow, *Biochemistry* **1992**, *31*, 3703–3708; b) S. E. Bennett, J. Kitner, *Nucleosides Nucleotides Nucleic Acids* **2006**, *25*, 823–842; c) A. G. Condie, Y. Yan, S. L. Gerson, Y. Wang, *PloS One* **2015**, *10*, e0131330; d) D. Boturyn, A. Boudali, J.-F. Constant, E. Defrancq, J. Lhomme, *Tetrahedron* **1997**, *53*, 5485–5492; e) H. Atamna, I. Cheung, B. N. Ames, *Proc. Natl. Acad. Sci.* **2000**, *97*, 686–691.
[20] T. Wai, D. Teoli, E. A. Shoubridge, *Nat. Genet.* **2008**, *40*, 1484–1488.
[21] J. B. Stewart, P. F. Chinnery, *Nat. Rev. Genet.* **2015**, *16*, 530–542.
[22] D. Ballmaier, B. Epe, *Toxicology* **2006**, *221*, 166–171.
[23] C. Furihata, *Gene. Environ.* **2015**, *37*, 21.
[24] C.-S. Lin, L.-T. Liu, L.-H. Ou, S.-C. Pan, C.-I. Lin, Y.-H. Wei, *Oncology reports* **2018**, *39*, 316–330.
[25] B. van Loon, E. Markkanen, U. Hübscher, *DNA Repair* **2010**, *9*, 604–616.
[26] J. W. Hanes, D. M. Thal, K. A. Johnson, *J. Biol. Chem.* **2006**, *281*, 36241–36248.
[27] Y.-S. Lee, W. D. Kennedy, Y. W. Yin, *Cell* **2009**, *139*, 312–324.
[28] S. U. Liyanage, R. Hurren, V. Voisin, G. Bridon, X. Wang, C. Xu, N. MacLean, T. P. Siriwardena, M. Gronda, D. Yehudai, *Blood* **2017**, *129*, 2657–2666.
[29] S. Cadenas, *Biochimica et Biophysica Acta (BBA)* **2018**, *1859*, 940–950.
[30] Y.-k. Tahara, D. Auld, D. Ji, A. A. Beharry, A. M. Kietrys, D. L. Wilson, M. Jimenez, D. King, Z. Nguyen, E. T. Kool, *J. Am. Chem. Soc.* **2018**, *140*, 2105–2114.
[31] P. Mishra, D. C. Chan, *Nat. Rev. Mol. Cell Biol.* **2014**, *15*, 634–646.
[32] a) M. Martinez-Diez, G. Santamaría, Á. D. Ortega, J. M. Cuezva, *PloS one* **2006**, *1*, e107; b) H.-C. Lee, Y.-H. Wei, *Int. J. Biochem. Cell Biol.* **2005**, *37*, 822–834.
[33] M. Trinei, I. Berniakovich, P. G. Pelicci, M. Giorgio, *Biochimica et Biophysica Acta (BBA)* **2006**, *1757*, 624–630.
[34] D. Ji, A. A. Beharry, J. M. Ford, E. T. Kool, *J. Am. Chem. Soc.* **2016**, *138*, 9005–9008.
[35] Y. Yin, F. Chen, *Acta Pharm. Sin. B* **2020**, *10*, 2259.
[36] a) A. M. Fleming, C. J. Burrows, *Free Radic. Biol. Med.* **2017**, *107*, 35–52; b) R.-Y. Zhu, C. Majumdar, C. Khuu, M. De Rosa, P. L. Opresko, S. S. David, E. T. Kool, *ACS Cent. Sci.* **2020**, *6*, 1735–1742.
[37] C. T. Coey, A. C. Drohat, *Methods in enzymology* **2017**, *592*, 357–376.
[38] A. G. Raetz, Y. Xie, S. Kundu, M. K. Brinkmeyer, C. Chang, S. S. David, *Carcinogenesis* **2012**, *33*, 2301–2309.
[39] D. Mangal, D. Vudathala, J.-H. Park, S. H. Lee, T. M. Penning, I. A. Blair, *Chem. Res. Toxicol.* **2009**, *22*, 788-797.
[40] a) B. Van Houten, G. A. Santa-Gonzalez, M. Camargo, *Curr. Opin. Toxicol.* **2018**, *7*, 9–16; b) S. Adar, J. Hu, J. D. Lieb, A. Sancar, *Proc. Natl. Acad. Sci.* **2016**, *113*, E2124; c) M. A. Spassova, D. J. Miller, A. S. Nikolov, *Oxid. Med. Cell. Longev.* **2015**, *2015*, 764375.
[41] Y. W. Jun, H. R. Kim, Y. J. Reo, M. Dai, K. H. Ahn, *Chem. Sci.* **2017**, *8*, 7696–7704.
[42] J.-L. Yang, L. Weissman, V. A. Bohr, M. P. Mattson, *DNA Repair* **2008**, *7*, 1110–1120.
[43] Y. J. Reo, Y. W. Jun, S. W. Cho, J. Jeon, H. Roh, S. Singha, M. Dai, S. Sarkar, H. R. Kim, S. Kim, *Chem. Commun.* **2020**, *56*, 10556–10559.
[44] R. X. Santos, S. C. Correia, X. Zhu, M. A. Smith, P. I. Moreira, R. J. Castellani, A. Nunomura, G. Perry, *Antioxid. Redox. Signal.* **2013**, *18*, 2444–2457.
[45] E. W. Englander, Z. Hu, A. Sharma, H. M. Lee, Z. H. Wu, G. H. Greeley, *J. Neurochem.* **2002**, *83*, 1471–1480.
[46] D. Liu, D. L. Croteau, N. Souza-Pinto, M. Pitta, J. Tian, C. Wu, H. Jiang, K. Mustafa, G. Keijzers, V. A. Bohr, *J. Cereb. Blood Flow Metab.* **2011**, *31*, 680–692.

10.1002/anie.202111829

WILEY-VCH

RESEARCH ARTICLE

## Entry for the Table of Contents

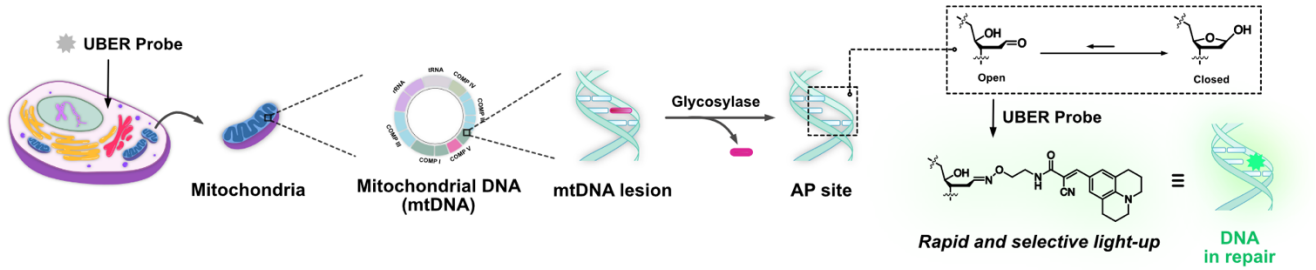


A light-up fluorescent probe (UBER) that reacts rapidly with AP sites resulted from DNA base excision repair (BER) visualizes BER process of mitochondrial DNA (mtDNA) in cells. Monitoring mtDNA BER process in cells over time illuminated the time lag between the initiation of oxidative stress and the initial step of DNA repair, along with the effect of DNA defensive enzymes, MTH1 and OGG1.

Institute and/or researcher Twitter usernames: @koolchemistry